A 1 GHz CMOS RF Front-End IC for a Direct-Conversion Wireless Receiver

Ahmadreza Rofougaran, James Y.-C. Chang, Maryam Rofougaran, and Asad A. Abidi, *Fellow, IEEE*

***Abstract*—An integrated low-noise amplifier and downconversion mixer operating at 1 GHz has been fabricated for the first time in 1 μm CMOS. The overall conversion gain is almost 20 dB, the double-sideband noise figure is 3.2 dB, the IIP3 is +8 dBm, and the circuit takes 9 mA from a 3 V supply. Circuit design methods which exploit the features of CMOS well suited to these functions are in large part responsible for this performance. The front-end is also characterized in several other ways relevant to direct-conversion receivers.**

I. Introduction

MOTIVATED by the growing needs for low-power and low-cost wireless transceivers, mainstream IC technologies are competing to integrate more RF functions onto a single chip. Bipolar circuits dominate integration at 1 GHz today, followed by GaAs IC's. As recent results demonstrate, CMOS too is a viable contender in this frequency range [1]–[6]. If CMOS is shown to perform in certain important respects as well as circuits in other established technologies, and it successfully merges analog and digital blocks, its use at RF may become as compelling as it is in baseband circuits.

To date, most research on CMOS RF circuits shows the feasibility of elementary RF building blocks, such as standalone tuned amplifiers [1], mixer IC's [2], [5], and oscillators [7]. The next development step calls for the integration of these building blocks into subcells, comparable in function to currently available small-scale RF IC's in bipolar or GaAs technology. The most common example of such an IC is an RF low-noise amplifier (LNA) combined with a downconversion mixer, often labeled the *front-end* for an RF receiver. Integrated front-ends are widely used because they combine all the RF signal processing on one chip, often requiring only a small overhead of off-chip components, and they produce an amplified signal translated down to a conveniently low intermediate frequency (IF) at the output. Thereafter, it is relatively simple to implement IF and baseband circuits for the rest of the receiver. The work reported here is the first implementation of a 1 GHz front-end in CMOS.

The front-end of a wireless receiver must meet several exacting specifications. First is *sensitivity*. The input noise of the front-end must be sufficiently low to enable it to detect weak input signals. The front-end gain must be high enough to overcome the noise contributions of later circuits, which may otherwise degrade the receiver sensitivity. Second, a front-end with a wide *input dynamic range* can tolerate large undesired signals nearby in frequency to a weak desired signal, which may otherwise, through intermodulation distortion, create energy at frequencies overlapping the desired channel. Third, the *RF input impedance* of the front-end must be a good match to the antenna characteristic impedance over the frequency band of interest.

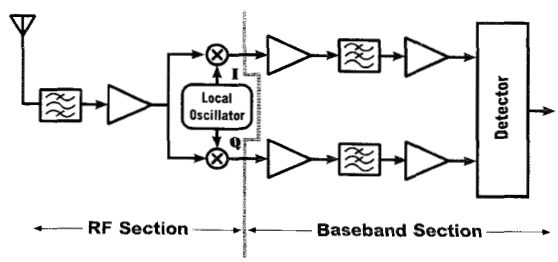


Fig. 1. A direct-conversion receiver suitable for FSK modulation.

The LNA and mixer together determine the performance of the front-end. For instance, although a large LNA gain is desirable as mentioned above, too large a gain may overload the mixer and compromise dynamic range. On the other hand, the gain must be large enough to overcome the fundamentally higher mixer noise. It is also desirable to connect the LNA in some simple way to the mixer input, without a power-hungry RF buffer. The front-end design is influenced by its intended use, as discussed below. Therefore, good performance is only obtained through careful *co-design* of the front-end building blocks.

This front-end is intended for a direct-conversion, or zero-IF, frequency-shift keying (FSK) receiver [8], which simplifies how the blocks are connected together (Fig. 1). In a superheterodyne receiver, a passive filter—usually a second preselect filter of the type connected to the antenna—follows the LNA [9] to suppress the amplifier noise in the image of the RF input band, where there is no signal. Without this filter, the downconverted signal must contend with downconverted noise from both the signal-bearing and the idle sidebands. In a direct-conversion receiver, on the other hand, the local oscillator (LO) is centered in the desired channel, so useful signal energy, and noise, occupy *both* upper and lower sidebands. As there is now no idle sideband to be filtered, the LNA is directly connected to the downconversion mixer. Therefore, when a

Manuscript received January 23, 1996; revised March 5, 1996. This work was supported by the U.S. Advanced Research Projects Agency, Rockwell International, Texas Instruments, Harris Semiconductor, Advanced Micro Devices, Hewlett-Packard Company, and the State of California MICRO Program.

The authors are with the Integrated Circuits & Systems Laboratory, Electrical Engineering Department, University of California, Los Angeles, CA 90095-1594 USA.

Publisher Item Identifier S 0018-9200(96)04472-1.

0018–9200/96$05.00 © 1996 IEEE

ParkerVision Exhibit 2032
TI v. ParkerVision - IPR2024-00934

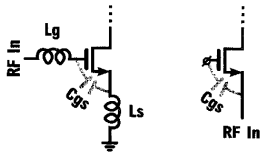


Fig. 2. Candidate FET LNA input stages. (a) Common-source stage, with lossless matching network. (b) Common-gate stage.

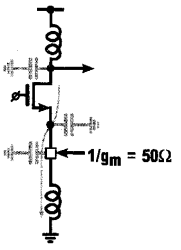


Fig. 3. Low-noise amplifier with tuned load and an off-chip tuning inductor at the input port.

modulation such as FSK permits use of direct-conversion [10], the receiver may be integrated with a need for very few off-chip components. There are several advantages to this, mainly small physical volume, less wasted power in buffering high-frequency signals off-chip, and lower assembly costs. However, the receiver requires a vector baseband signal path, consisting of two branches downconverted in quadrature to prevent the signal-bearing image sidebands from aliasing on one another.

II. Circuit Design

A. Low-Noise Amplifier

The LNA must simultaneously attain high RF gain, low input noise, and a good input match to 50 Ω. These requirements are often interdependent in a simple circuit, and may require iterative design for all to be fulfilled. The following discussion on a CMOS LNA design covers input impedance matching first, then input noise, and finally voltage gain.

The gate of a FET fabricated in 1-μm technology is capacitive to frequencies beyond 1 GHz.[1] However, a lossless *matching network*, consisting only of inductors and capacitors can transform the FET input into a pure resistance over some frequency band of interest. The most common matching network for FET's consists of a series feedback inductor, L_s, in the FET source, and another inductor, L_g, in series with the gate to tune out the capacitance $C_{\rm gs}$, resulting in an input resistance $g_m L_s/C_{\rm gs}$ where g_m is the FET transconductance [Fig. 2(a)] [11]. This method is preferred over resistor feedback because the matching network introduces no noise of its own. However, loss in practical inductors L_g and L_s will tend to degrade noise figure. With sufficiently good inductors, though, a noise figure well below 3 dB may be obtained with this technique, ultimately limited by such transistor imperfections as nonzero gate resistance.

When a noise figure of 3 dB is acceptable, as it is in our receiver, it is simpler to regulate the input impedance with a common-gate input stage [12] [Fig. 2(b)]. For the sake of discussion, first suppose that the load resistance at the drain is much less than the FET $r_{\rm ds}$, and that $g_m r_{\rm ds} \gtrsim 10$. Then the input resistance at the FET source is $1/g_m$. At 1 GHz, the FET $C_{\rm gs}$ and parasitic input capacitance, C_P, due to the bonding pads and external strays significantly shunt this resistance. Therefore, to achieve a good impedance match, the size and bias of the FET are selected for $1/g_m = 50\ \Omega$, and an inductor tunes out the shunt capacitance by parallel resonance in a frequency band around 1 GHz. As the capacitance at the LNA input is to be tuned, it makes good sense to do so with a grounded off-chip low-loss inductor, which also carries the LNA bias current.

Fortuitously, a FET with a small-signal channel resistance of 50 Ω produces a lower thermal noise current than a linear resistor of the same value [13]. The noise current spectral density in the FET is $4kT\gamma g_m A^2$/Hz, where $\gamma \simeq 0.67$ owing to the distributed inversion layer. Thus, ruling out any other noise sources in a matched LNA, the noise figure due to the FET alone is $10\log 1.67 = 2.2$ dB. In a short-channel FET biased at unfavorable conditions, hot-electron effects may augment this [14] to raise the noise figure. Flicker noise in the FET is unimportant at RF.

A tuned load peaks the frequency response of the LNA in the band of interest (Fig. 3), in effect transforming the inherent lowpass characteristic of the amplifier to a bandpass. The load also helps to reject out-of-band signals and noise. However, the LNA passband is seldom sufficiently flat and narrow for RF *preselection*, that is, to suppress image channels and out-of-band interferers. Rather, a sharply tuned discrete filter, such as SAW or dielectric resonator, is inserted before the LNA for this purpose. Discrete filters usually operate at a characteristic impedance of 50 Ω or 75 Ω. As explained above, no preselect filter need follow this LNA, nor the RF buffer required to drive the filter.

The tuned load, therefore, comprises an inductor resonating with the FET drain capacitance, C_D, and the sum, C_P, of the input capacitance of the subsequent downconversion mixer and any other parasitics. Another advantage of the common-gate stage is that the somewhat large $C_{\rm GD}$ of the FET returns its current to a fixed bias, rather than to the input node as it would in a common-source amplifier. This current undergoes rapid phase-shifts with frequency in an RF tuned amplifier, and makes it difficult to design an input matching circuit.

The inductance, L, to tune this total capacitive load to the resonant frequency ω_0, in our case 2π Grad/s, is

$$L = 1/\omega_0^2(C_D + C_P). \tag{1}$$

In most modern FET's, the drain junction capacitance $C_D \simeq C_{\rm GS}$. Furthermore, the unity-current gain frequency, $\omega_T =$

[1] This assumes the FET is laid out sensibly. The gate resistance of a FET with a certain channel width is lowered by an interdigitated gate, whereas without such a layout, this resistance may dominate the FET input impedance at high frequencies.

ParkerVision Exhibit 2032
TI v. ParkerVision - IPR2024-00934

g_m/C_{GS}. The inductance may then be expressed as

$$L = \frac{1}{\omega_0^2(g_m/\omega_T + C_P)}. \quad (2)$$

If inductor loss, as modeled by a series resistance R_S, limits the impedance of the tuned load at resonance, then using (2), the voltage gain of the common-gate stage is

$$\text{Gain} = g_m \frac{(\omega_0 L)^2}{R_S} = \frac{\omega_T}{1 + \omega_T C_P/g_m} \frac{L}{R_S}. \quad (3)$$

This form makes it clear which parameters are within the circuit designer's reach to determine RF gain. ω_T mainly depends on FET channel length, but is also controlled by gate bias. However, even with infinite ω_T, parasitic-related quantities will limit the maximum achievable gain to

$$\text{Max Gain} = \min\left(\frac{g_m}{C_P}\frac{L}{R_S}, g_m r_{DS}\right). \quad (4)$$

In the common-gate amplifier, the desired input impedance sets g_m. Thus, a large parasitic capacitance at the drain means a smaller achievable gain, unless the loss in the load inductor is somehow lowered to boost the gain. The relative quality of the inductor, L/R_S, depends on how it is physically realized, and there are limits to how large this may be in practice. For instance, at 1 GHz the L/R_S is 4 nH/Ω for a discrete 10 nH chip inductor meant for RF applications [15]. This argues for an on-chip inductor load, because it is unlikely that a discrete off-chip inductor can overcome, simply because of a higher quality, the RF gain loss due to the large parasitic capacitance of the bond pads, bondwires, package leads, and board traces.

The LNA fulfills its specifications at the price of power dissipation. At low values of gate drive voltage, long-channel FET laws fairly well describe the dependence of bias current, I_D, on the transconductance

$$I_D = \frac{1}{2} g_m (V_{GS} - V_t). \quad (5)$$

Similarly, at low gate drives, the ω_T of a FET theoretically follows the dependence

$$\omega_T = \frac{g_m}{C_{GS}} = \frac{\mu}{1 + \theta(V_{GS} - V_t)} \frac{(V_{GS} - V_t)}{L^2} \quad (6)$$

where θ captures how the inversion-layer mobility, μ, degrades with gate electric field [16]. While (5) is readily verified by measurement, there is little data in the literature on CMOS ω_T to validate (6). Therefore, the s-parameters of a single, large 1-μm NFET were characterized on a Cascade™ probe station, from which ω_T was deduced. The measured data (Fig. 4) shows that $\omega_T = 2\pi f_T$ conforms closely to (6) in the $V_{GS} - V_t$ range of interest. This curve serves as an important design aid.

Using (2), the load inductance may be calculated which tunes the LNA to a certain frequency in the absence of any significant parasitics. For instance, if the FET is biased at an f_T of 5 GHz, then the LNA requires a 40 nH inductor load to achieve a peak at 1 GHz in its frequency response. The inductor may be implemented on-chip as a square spiral in Metal-2, with the return conductor in Metal-1. Greenhouse's formula accurately specifies how the inductance grows with the number of turns [17], while the series resistance accumulates with the number of squares of metal comprising the spiral [Fig. 5(a)]. The spiral grows outwards from a 140 μm square hole in the middle. Any turns within the hole would enclose relatively little magnetic flux, but would contribute a nonnegligible unwanted resistance. These curves show that in the inductance range of 40 to 50 nH, the relative quality, L/R_S, of the spiral is about 0.7 nH/Ω. It is seen from (3), (5), and Fig. 4 that the LNA may achieve a gain as large as 20 dB at 1 GHz in the absence of parasitic capacitance, while drawing 1.5 mA of current per FET.

The main impediment to a practical implementation of the tuned amplifier arises from the parasitic capacitance of a 50 nH

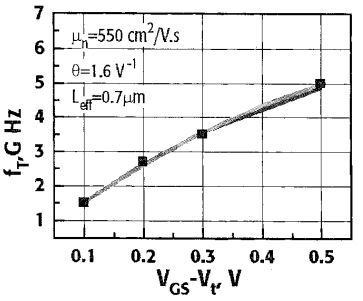


Fig. 4. Measured f_T versus $V_{GS} - V_t$ for MOSIS 1-μm NMOSFET (points) fitted to simple expression (line).

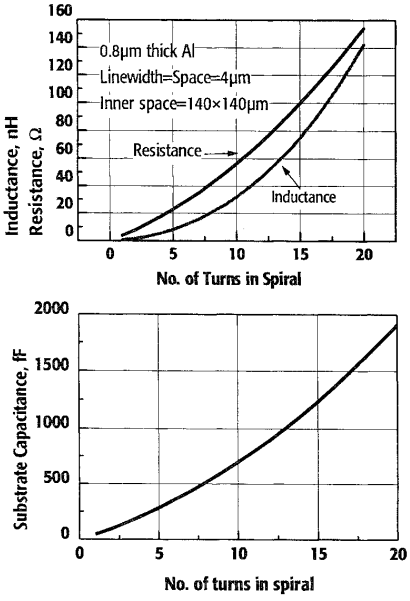


Fig. 5. Design curves for square spiral on-chip inductor. (a) Inductance and resistance of spiral versus number of turns and (b) capacitance of inductor (assuming it is an equipotential) to substrate through 1 μm thick field oxide.

ParkerVision Exhibit 2032
TI v. ParkerVision - IPR2024-00934

spiral inductor to the semiconductor substrate. This is so large through the typical 1 μm-thick field oxide [Fig. 5(b)] that the spiral self-resonates at 700 MHz, and at 1 GHz appears as a capacitive, rather than inductive, load on the LNA. This is why it is generally believed that medium- to large-value inductors may only be integrated on semi-insulating substrates, while on a standard silicon substrate inductors no larger in value than 5 to 10 nH are usable at 1 GHz [18].

In earlier work, we have described a method to eliminate the parasitic capacitance under the spiral inductor by selectively removing the underlying silicon substrate [1]. This leaves the spiral encased in a layer of oxide suspended above an air-gap. Inductors as large as 100 nH may be fabricated in CMOS, whose self-resonance frequency, now limited by the small fringing capacitance through the air gap to the distant ground plane, lies beyond 2 GHz. This maskless, post-fabrication etching of the substrate does not require any foundry modifications in the 1-μm CMOS process available through MOSIS. Via holes which will expose the surface of the silicon after fabrication and passivation surround the spiral. A selective etchant removes the exposed silicon at a much higher rate than it does oxide and metal. After sufficient exposure to the etchant, a deep cavity forms under the inductor, while the remaining active area on the chip is left intact. A passivating coat protects the exposed silicon on the sides and back of the chip from inadvertent etching.

The substrate was removed in the earlier work by a liquid-phase, anisotropic etchant [1], resulting in a spiral inductor surrounded by large trapezoidal openings, and attached by four oxide bridges to the rest of the CMOS substrate. This has since been replaced by a gas-phase, isotropic etchant. Through small circular openings surrounding the spiral, the etchant now excavates hemispherical pits whose radius increases with exposure time. Etching is stopped when the multiple pits coalesce into one large pit with a depth of roughly half of one side of the spiral (Fig. 6). This suspended inductor enables wholly-integrated RF components in CMOS. In addition to the LNA, it is also used in the local oscillator, power amplifier, and even as a low quality bandpass filter. As a survey in a recent publication shows [19], no simpler method has yet been found to realize large-value integrated inductors.

It was assumed in the earlier analysis that the impedance, Z, of the LNA tuned load is much less than the FET $r_{\rm ds}$. When this is not so, the expressions for the gain and input impedance must be modified to

$$\text{Gain} = \frac{g_m Z}{\left(1+\frac{Z}{r_{\rm ds}}\right)}; \qquad r_{\rm in} = \frac{1}{g_m}\left(1+\frac{Z}{r_{\rm ds}}\right). \tag{7}$$

The complete LNA is a balanced circuit (Fig. 7). A power-conserving, passive balun converts a single-ended antenna signal into a balanced input drive to the LNA. A printed-circuit balun may even be integrated into the transceiver case. The bias, VG, at the common-gate FET's regulates the LNA input impedance. An on-chip scaled-down replica circuit stabilizes this impedance against variations in process and temperature as follows. An op-amp drives the VG bias voltage of the replica to servo the dc value of $1/g_m$ to an off-chip reference

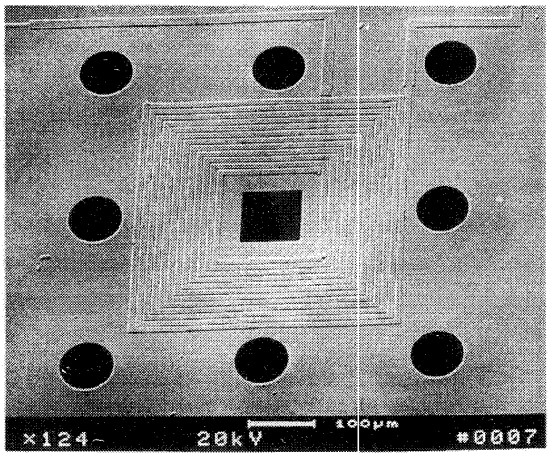


Fig. 6. Suspended 50 nH spiral inductor over a hemispherical cavity etched underneath through surrounding via holes.

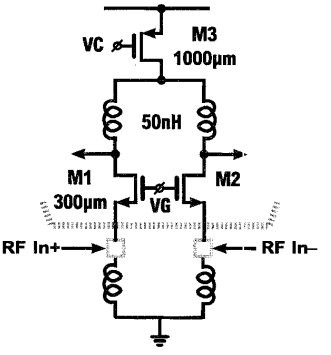


Fig. 7. Low-noise amplifier circuit diagram.

resistance, and the same voltage is then applied to the main LNA, thereby regulating its input impedance to within the FET matching in the replica and the main circuits. As the feedback loop bandwidth is well below 1 MHz, the op-amp does not contribute any RF noise. The inductor loads on each half of the circuit share a common top-node, which connects to the 3 V power supply through a triode-region PFET. By adjusting the gate voltage, VC, the dc voltage drop across this PFET resistor may be changed, and this sets the dc level at the LNA output.

The LNA FET's are biased at $V_{\rm GS}-V_t = 0.35$ V, and drain 2.2 mA each. Taking into account the capacitive load of the mixer, the LNA requires 50 nH load inductors to obtain a peak at 1 GHz in its frequency response. From (4) and Fig. 4, this means that in the absence of parasitics ($C_P = 0$), the peak RF gain is at most 26 dB.

B. Downconversion Mixer

The amplified signal at the LNA output is converted down in frequency for further amplification, channel-select filtering,

ParkerVision Exhibit 2032
TI v. ParkerVision - IPR2024-00934

and detection. The frequency mixer is an integral part of the RF front-end.

There are two fundamentally different ways to implement a mixer in CMOS. The first, somewhat unconventional method, uses a MOSFET as a wideband analog switch. A passive track-and-hold circuit, consisting of a 1-μm FET switch and a grounded capacitor, is designed for a track-mode bandwidth of greater than 1 GHz. This follows the waveform of a modulated 1 GHz carrier and samples it at a much lower rate, which must be at least twice the *modulation* bandwidth. An op-amp feedback circuit clocked at this low sample rate buffers the held output, and removes signal-dependent charge injected by the switch. When the sample rate is an integer submultiple of the carrier frequency, the interpolated samples directly downconvert the RF signal to dc. A prototype evaluated at a 900 MHz RF [2] shows very good linearity, but fundamentally suffers from a large noise figure, because while tracking the narrowband signal, it also tracks and aliases wideband noise. This, and the difficulty of buffering such a switched mixer to the inductive load of an integrated LNA, make it inappropriate in a sensitive receiver.

The second, more conventional, mixer resembles the Gilbert analog multiplier. It consists of a linear RF voltage-to-current (V-I) converter, or RF transconductor, whose output current is commutated by the local oscillator (LO). As commutation conserves the total current, it downconverts a fraction of the RF current to the IF, and the remaining RF current upconverts around one or more harmonics of the LO. The voltage conversion-gain of the active mixer is independently set by choice of the transconductance and load resistance. The internal current conversion-loss penalizes mixer noise, as is analyzed in a later section.

A good mixer is highly linear, and its input-referred noise does not overwhelm the amplified noise of the preceding LNA. The mixer handles larger signals than the LNA, and therefore its nonlinearity must be lower by at least a factor of the LNA gain if it is not to become the bottleneck to receiver dynamic range. This is why the following discussion concentrates on mixer nonlinearity, as the LNA, with the choice of bias voltages, is not the bottleneck to front-end linearity.

Third-order intermodulation distortion in a double-balanced mixer may cause two large adjacent-channel signals to create energy at spurious frequencies coincident with a weak desired channel. The linearity of a front-end is specified by the input-referred third-order intercept point (IIP3) [20]. Often this is set by the static and dynamic nonlinearity in the RF V-I converter of the mixer, or by the static nonlinearity in the mixer load.

Linear MOS transconductance circuits have been studied extensively in the context of continuous-time active filters [21] operating at frequencies up to tens of MHz. These circuits exploit the property that the dominant second-order nonlinearity in a MOSFET circuit cancels in balanced differential inputs and outputs. For instance, if two identical common-source FET's conforming to the classic long-channel I-V characteristics are biased at some V_{GS} [Fig. 8(a)] and excited differentially by a large signal V_{in} whose amplitude is less

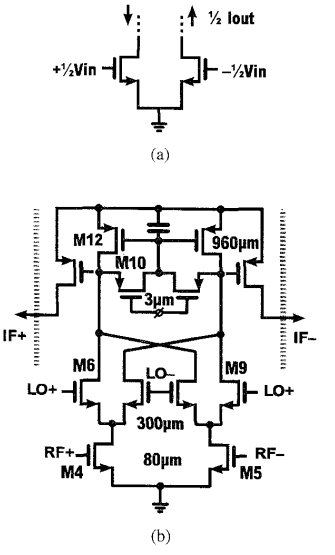


Fig. 8. (a) Linear MOS transconductor. (b) Downconversion mixer circuit diagram.

than $2(V_{GS} - V_t)$, then the differential output current

$$I_{out} = \mu C'_{ox}(W/L)(V_{GS} - V_t)V_{in} \tag{8}$$

depends *linearly* on V_{in}, and the bias $V_{GS} - V_t$ sets the transconductance [22].

Residual third-order nonlinearity produces a small distortion in the transconductor. Its large signal handling is limited by clipping when an input swing of $V_{GS} - V_t$ turns off one of the FET's in the circuit. These sources of static nonlinearity are expected to govern the mixer up to and beyond 1 GHz, as no significant nonquasi-static effects are likely to set in given the short carrier transit time in the 1-μm channel. Dynamic nonlinear currents which grow with frequency will flow in any voltage-dependent FET capacitance and might even become the significant form of distortion at 1 GHz. The MOSFET, however, is benign in this respect, as its main capacitance, C_{GS}, is relatively independent of bias for $V_{GS} > V_t$ and behaves like a linear capacitor in the saturation region of operation.

The MOS downconversion mixer is a balanced circuit [Fig. 8(b)] comprising a linear common-source FET transconductor (as opposed to a differential pair in the bipolar Gilbert multiplier), four commutating FET switches, and a high-swing load consisting of a center-tapped FET resistor across pull-up current sources. Common-mode feedback from the center tap biases the current sources at a well-defined voltage. The LNA output is directly connected into the differential mixer input.

The mixer attains its peak conversion gain when a sinewave of at least +5 dBm (1 V ptp) is applied to the commutating switches $M6$–$M9$. This also lowers the total front-end noise figure. While it is obvious that incomplete commutation leads to conversion loss, what may not be evident is how it also degrades noise figure. The transconductor FET's and the loads clearly contribute noise in the mixer. In addition, the

ParkerVision Exhibit 2032
TI v. ParkerVision - IPR2024-00934

commutating switch FET's also contribute noise at discrete time intervals over the switching cycle. The time-varying aspects of the circuit must be understood to estimate the magnitude of this contribution. Over most of the duty cycle, one FET in each switched pair appears as a resistor in series with transconductor, while its companion FET is OFF. The series FET contributes very little noise, determined only by the finite output impedance of the transconductor FET's at 1 GHz. However, during a zero-crossing of the LO, the two companion switch FET's carry comparable drain currents, and act, for the purposes of noise analysis, like a differential pair amplifier. They then contribute a short burst of balanced noise current to the mixer load with a spectral density proportional to the switch FET transconductance, elevating the average mixer output noise [23]. A larger LO drive to the mixer forces zero crossings with a greater slope, and as the switches now dwell for a shorter fraction of the period in the high noise condition, the overall mixer noise is lowered.

It is a good assumption that under large LO drive, the mixer commutates the RF transconductance current with a square wave. Simple expressions may now be derived for the mixer *conversion gain* and its equivalent *input noise*. Referring to Fig. 8(b), suppose a unit sinusoidal input voltage of frequency ω_{RF} is linearly converted to a current, and commutated by the switches at ω_{LO}, which amounts to multiplying the sinusoidal current by a square wave, $\mathrm{sq}(\omega_{\mathrm{LO}}t)$, alternating between $+1$ and -1. The current flowing into the loads, I_{IF}, is then

$$\begin{aligned} I_{\mathrm{IF}} &= g_{m4}\sin\omega_{\mathrm{RF}}t \times \mathrm{sq}\omega_{\mathrm{LO}}t \\ &= g_{m4}\sin\omega_{\mathrm{RF}}t \times (4/\pi)\left(\sin\omega_{\mathrm{LO}}t + \frac{1}{3}\sin 3\omega_{\mathrm{LO}}t + \cdots\right) \\ &= (2/\pi)g_{m4}\cos(\omega_{\mathrm{RF}} - \omega_{\mathrm{LO}})t \end{aligned} \tag{9}$$

where the square wave is expanded as a Fourier series, and the term containing the downconverted frequency at $\omega_{\mathrm{RF}} - \omega_{\mathrm{LO}}$ is retained. Equation (9) shows a current conversion loss of at least $2/\pi(=0.64)$ through this mixer. The overall mixer voltage gain is

$$\text{Mixer Gain} = (2/\pi)g_{m4}R_L \tag{10}$$

which may be adjusted to any reasonable value by the load resistance, R_L, attached to the low-frequency output node. Noise due to the mixer loads is referred to the input in the following way: the noise current is divided by the *conversion loss*; the noise spectrum is *translated* from ω_{IF} to ω_{RF}; and the noise is distributed equally between *two image sidebands* around ω_{LO} which will downconvert to the same ω_{IF}.[2] Suppose that the transconductor and load FET's $(M12, M13)$ [Fig. 8(b)] produce only thermal (white) noise, that the commutating switch FET's contribute no noise, and that the noise due to the spectral density FET resistor loads $(M10, M11)$ is negligible. Then the noise referred to the mixer input is

$$\hat{v}_n^2 = 4kT\gamma\left(\frac{1}{g_{m4}} + \frac{1}{2}\left(\frac{\pi}{2}\right)^2\frac{g_{m12}}{g_{m4}^2}\right). \tag{11}$$

[2]This assumes that the conversion gain is equal from both sidebands, which is a very good approximation for low ω_{IF}.

As $M4$ and $M12$ share the same bias current, it follows that with the FET sizes used in this circuit

$$\frac{g_{m12}}{g_{m4}} = \sqrt{\frac{\mu_P W(M12)}{\mu_N W(M4)}} \approx 2. \tag{12}$$

From (11) and (12), this means that noise voltage referred at the mixer input is 1.8× larger than if the input FET's $(M4)$ were the sole source of noise. In the case of direct-conversion where $\omega_{\mathrm{IF}} = 0$, flicker noise in the load will further elevate, indeed dominate, the mixer input noise.

The NFET's at the mixer input are biased at $V_{\mathrm{GS}} - V_t = 0.75$ V, and drain 2.4 mA each from the 3 V supply. From (11), the referred input noise voltage level of this mixer is about 3.5 nV/$\sqrt{\text{Hz}}$, which is overwhelmed by LNA output noise of roughly 12 nV/$\sqrt{\text{Hz}}$ due to its own FET's. We conclude that the mixer does not appreciably degrade the noise figure of the front-end.

The $V_{\mathrm{GS}} - V_t$ of the pull-up PFET current sources is also 0.75 V, and as the signal level at the mixer input is 1.4× at the output, clipping will commence at the transconductor input. It may be shown with straightforward calculus that the rms value of a sinewave falls by 1 dB when it is clipped to 81% of its undistorted amplitude. This predicts that at the above bias points, the conversion gain of the front-end will compress by 1 dB due to clipping at the mixer input when a balanced sinewave of about −4 dBm is applied to the LNA.

For the purposes of standalone testing, open-drain PFET's connect to the mixer output to drive off-chip loads. They require an additional bias current, which is high enough to enable them to drive a large power level into the 50 Ω impedance of measuring instruments. However, in the intended on-chip use, they will be radically scaled down in size to drive a small capacitive load. The signal from the mixer output onwards is at a low or even a zero IF, so considerations of noise, not bandwidth, set the power dissipation in the subsequent stages.

III. Implementation and Measurements

A. Layout Issues

The RF front-end, comprising the LNA and mixer, is laid out for fabrication in a standard two-level metal, 1-μm CMOS process offered by MOSIS. The two on-chip spiral inductors in the LNA dominate the 1.3 × 2 mm active area of the die (Fig. 9). There are two features of note on this layout. First, circular via-holes surround the inductors to expose the silicon substrate after fabrication and passivation. Second, the LNA input pads are unusual. The standard MOSIS pad consists of 100-μm squares of Metal 2 and Metal 1 shorted together. This pad is, however, unsuitable for RF applications, because it is capacitively coupled through the oxide to the nonzero spreading resistance of the grounded silicon substrate. At 1 GHz, the pad impedance is mainly resistive and about 50 Ω. This parasitic resistance upsets the input impedance matching, but more seriously, it is a significant source of thermal noise. In fact, due to the pad alone, the LNA noise figure would

ParkerVision Exhibit 2032
TI v. ParkerVision - IPR2024-00934

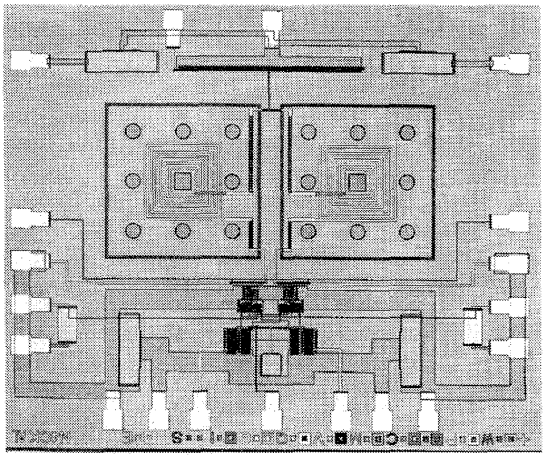


Fig. 9. Die photograph of front-end IC, consisting of LNA and downconversion mixer.

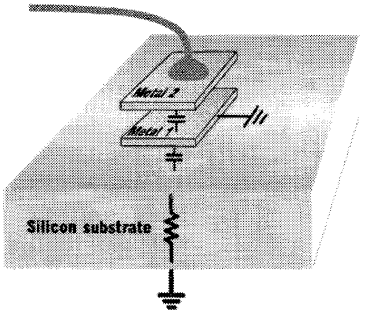
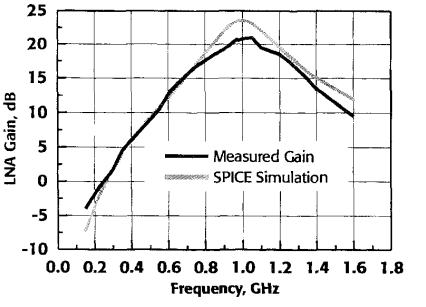


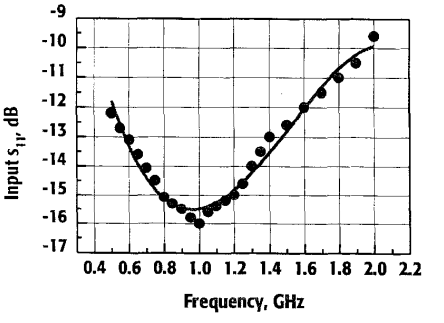
Fig. 10. Structure of RF input pad to LNA. Metal 1 shields the input signal from spreading resistance of substrate.

be 3 dB before any FET noise is taken into account. This problem always appears on silicon substrates at RF, although its magnitude varies with substrate doping. It has been noted before in discrete RF bipolar transistors [24].

The pad is modified to shield the RF input from this parasitic resistance. Instead of shorting the two layers of metal, Metal 1 is connected to a high-frequency ground, and the RF input pad is composed of Metal 2 alone, which also routes the signal from the chip periphery to the input FET's (Fig. 10). The pad impedance is now purely the capacitance between Metal 2 and Metal 1, and is no longer a source of noise. The off-chip inductor tunes out the pad capacitance with the various other capacitances that appear at the input node. This is a satisfactory though fragile solution, in that the pad is more susceptible to damage through the weak intermetal dielectric during wirebonding, and it cannot tolerate the loading of standard electrostatic protection devices. An alternative is to short the two layers of metal, but then place a heavily diffused layer under them which is connected either to ground, or stays at virtual ground when a balanced signal is applied to adjacent pads.



(a)



(b)

Fig. 11. Measured characteristics of low-noise amplifier. (a) Gain versus frequency, compared with SPICE simulation. (b) Input reflection coefficient versus frequency.

B. Experimental Results

All the following measurements are made with the chip mounted in a ceramic microwave package, to which a low-loss, power-conserving balun applies a balanced RF stimulus from a single-ended signal source. A low frequency power-combiner converts the balanced output into a single-ended signal for measurement. In most cases, the LO is offset from the RF input to produce a 10 MHz IF, which makes it easy to use ac-coupled instruments. However, the circuit is also evaluated in selected ways as a direct-conversion front-end. The LNA frequency response [Fig. 11(a)] is deduced from measurements on the overall conversion gain, by accounting for the mixer gain from transient simulations. SPICE, with standard static FET models and a simple three-element inductor model [1], predicts the LNA response very well. The scattering parameter s_{11} measures the input reflection coefficient, and thus the quality of the LNA input impedance match [Fig. 11(b)]. An s_{11} of -16 dB at 1 GHz is satisfactory for many applications, and implies a net input resistance of about 70 Ω, consistent with the FET g_m.

Another relevant attribute of the front-end is its ability to handle large signals without harmful distortion. Two equal-strength, closely-spaced tones around 1 GHz are applied to the LNA, and the strength of the corresponding downconverted tones f_1, f_2 is measured, as well as the strength of the spurious tones at $2f_1 - f_2$ and at $2f_2 - f_1$ produced by third-order

ParkerVision Exhibit 2032
TI v. ParkerVision - IPR2024-00934

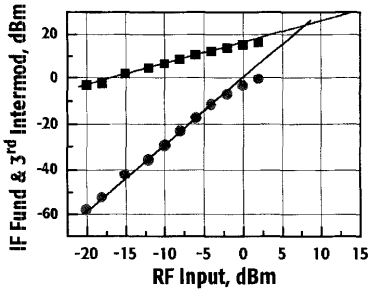
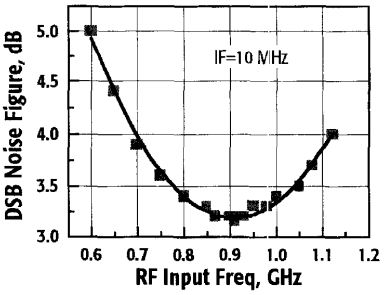


Fig. 12. Linearity of combined LNA and mixer, measured with two-tone input in LNA passband.

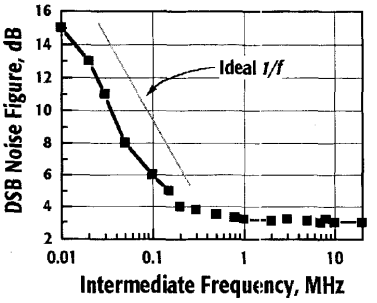
intermodulation. Whereas the main tones grow proportionally with the RF input amplitude, the distortion terms grow as the third power, and when extrapolated on logarithmic scales, the spurious tones grow as large as the main downconverted tones at an input of +8 dBm (Fig. 12). This is the input-referred third-order intercept point (IIP3). In practice, the LNA gain will collapse at a lower input, and although the IIP3 is the standard for specifying linearity, the 1-dB compression point better expresses the limits to linear operation. This is the input level, about −3 dBm for this circuit, at which conversion gain falls by 1 dB because of the onset of clipping. This is very close to the −4 dBm predicted above.

It is something of a challenge to measure the noise-figure of a direct-conversion receiver. A noise figure meter such as the HP 8970B can only measure noise at 10 MHz IF or above, yet its accuracy is unmatched by any other technique, because it simultaneously measures output noise and conversion gain. This meter is therefore first used to calibrate the noise-figure of the front-end at a 10 MHz IF. It measures the output IF noise levels in response to two reference levels of wideband noise spanning 10 MHz to 1.6 GHz. The correct double-sideband (DSB) noise figure is obtained when there is no RF preselect filter [20], because just as in the intended use for direct-conversion, *both* image sidebands around the LO contribute noise, as well as providing the input stimulus for gain measurement. Then, after grounding the input of the front-end through a 50 Ω resistor and applying a 1 GHz LO, the output noise spectral density is measured on a spectrum analyzer in the frequency interval from 0 to 10 MHz. If necessary, a wideband amplifier with a known gain and a bandwidth of more than 10 MHz is used to boost the front-end noise above the measurement floor of the spectrum analyzer. Any inaccuracy in the figure for double-sideband conversion-gain of the system is corrected by matching the input-referred noise spectral density at 10 MHz with the reading from the noise-figure meter. The noise-figure is then extrapolated to an arbitrary low frequency from the readings on the spectrum analyzer.

A DSB noise figure of 3.2 dB is measured on the noise-figure meter at a 10 MHz IF, which compares very favorably with the theoretical 2.9 dB noise figure of a single FET with a common-gate input impedance of 70 Ω [Fig. 13(a)]. In typical fashion of narrowband amplifiers, the noise figure rises as the



(a)



(b)

Fig. 13. Noise characteristics of front-end. (a) Direct noise figure measurement at 10 MHz IF. (b) Noise figure deduced from output noise spectrum at frequency offsets from zero IF.

matching deteriorates away from the tuned frequency of the input matching circuit—in this case, 0.9 GHz—and this is exacerbated by the declining LNA gain on either side of 1 GHz [Fig. 11(a)], when the mixer contributes more noise. Noise figure at low IF is deduced from spectrum analyzer measurements. Flicker noise now appears [Fig. 13(b)], contributed by the mixer pull-up current sources ($M12, M13$), and the PFET output buffers ($M14, M15$). The load FET's ($M10, M11$) do not carry a bias current, and therefore contribute no flicker noise. After direct downconversion in the intended receiver [8], the peaks in the spectrum of a 160 kb/s FSK signal lie at ±160 kHz, where flicker noise raises the front-end DSB noise figure to about 4.5 dB.

Second-order nonlinearity in the baseband section of a front-end also impairs a direct-conversion receiver [10], [25]. It detects the envelope of any unwanted AM signal in the LNA passband, and creates spurious energy at dc which overlaps, and may even overwhelm, the downconverted desired signal at dc. A fully-balanced circuit mitigates this to a large extent. The residual distortion is characterized by downconverting a 918 MHz carrier, which is amplitude-modulated at a 100% index by a 150 kHz tone, to an 18 MHz IF, and observing the spurious energy appearing at 150 kHz. The spurious tone grows with the second power of the carrier amplitude, and the magnitude of this nonlinearity is characterized by a second-order intercept, which is about +25 dBm referred to the input

ParkerVision Exhibit 2032
TI v. ParkerVision - IPR2024-00934

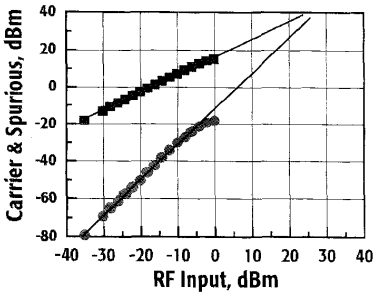


Fig. 14. Second-order intercept plots growth of detected envelope at dc versus AM signal strength. This is of importance in a direct-conversion receiver.

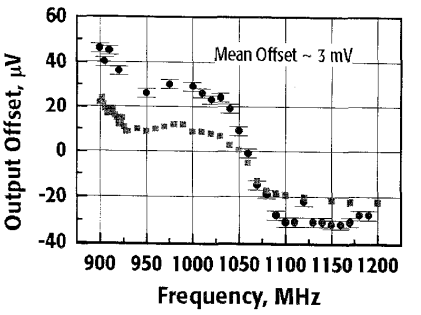


Fig. 15. Change in output dc offset as LO frequency is varied, as measured on two samples of the front-end IC.

TABLE I
RF FRONT-END IC SPECIFICATIONS

RF Input	1 GHz nominal (intended for 902-928 MHz)
LNA Gain	22 dB at 1 GHz
Mixer Gain	–3 dB
DSB Noise Figure	3.2 dB at 0.9 GHz 4.5 dB at 160 kHz
IIP3	+8 dBm
Current Drain	9 mA from 3 V
Technology	1-μm CMOS
Active area	1.3×2 mm

of this circuit (Fig. 14). This is much higher than the IIP3, and therefore is not expected to be a major limitation to receiver dynamic range.

Finally, the dc offset at the output of a zero-IF receiver appears in the middle of the downconverted signal spectrum. This offset will overwhelm the received signal, unless removed with capacitive coupling or nulled by some form of digital offset estimation [10]. These remedies are, however, only partly effective in the case of a *dynamic offset*. For instance, the offset may consist of a component due to self-downconversion of LO leakage [10], and in a frequency-hopped receiver such as ours [8], this will inevitably change with the instantaneous LO frequency. The output offset has been measured on two IC's over a broad sweep of the LO (Fig. 15). Interestingly, it remains constant to within 5 μV over the sweep from 950 to 1025 MHz, but then changes rapidly by up to 60 μV in the vicinity of 1050 MHz. Over the 902–928 MHz ISM band, the output offset changes by about 10 μV. The methods to remove offset described above cannot easily track the variations produced by an LO hopped by a pseudonoise code, but it is expected that the spectrum of the varying offset will be noiselike, and given the small size of the dynamic offset, it will only slightly raise the receiver noise floor. It is not clear what causes the offset to depend so sharply on frequency, but parasitic resonances on-chip and in the package are suspected.

IV. CONCLUSION

A 1 GHz RF front-end IC, comprising a low-noise amplifier and downconversion mixer, has been designed and fabricated in 1-μm CMOS. This will be integrated with the baseband portions of a direct-conversion receiver, all sharing a common CMOS substrate. We have applied a design style which uniquely exploits CMOS capability to implement key RF functions. Combining this with a new on-chip inductor technology, and taking into account the receiver architecture, we have demonstrated a fully integrated 1 GHz front-end in a modest 1-μm CMOS process (Table I) which, in some respects, exceeds the performance of similar circuits fabricated in other well-established RF technologies [26]. We are hopeful that this work opens new vistas for today's predominant IC technology, CMOS, in an application believed to have ubiquitous importance in the future.

REFERENCES

[1] J. Y.-C. Chang, A. A. Abidi, and M. Gaitan, "Large suspended inductors on silicon and their use in a 2-μm CMOS RF amplifier," *IEEE Electron Device Lett.*, vol. 14, no. 5, pp. 246–248, 1993.
[2] P. Y. Chan, A. Rofougaran, K. A. Ahmed, and A. A. Abidi, "A highly linear 1-GHz CMOS downconversion mixer," in *European Solid-State Circuits Conf.*, Sevilla, Spain, 1993, pp. 210–213.
[3] M. Rofougaran, A. Rofougaran, C. Olgaard, and A. A. Abidi, "A 900 MHz CMOS RF power amplifier with programmable output," in *Symp. on VLSI Circuits*, Honolulu, 1994, pp. 133–134.
[4] A. Rofougaran, J. Y.-C. Chang, M. Rofougaran, S. Khorram, and A. A. Abidi, "A 1 GHz CMOS RF front-end IC with wide dynamic range," in *European Solid-State Circuits Conf.*, Lille, France, 1995, pp. 250–253.
[5] J. Crols and M. Steyaert, "A 1.5 GHz highly linear CMOS downconversion mixer," *IEEE J. Solid-State Circuits*, vol. 30, no. 7, pp. 736–742, 1995.
[6] ——, "A fully integrated 900 MHz CMOS double quadrature downconverter," in *Int. Solid-State Circuits Conf.*, San Francisco, pp. 136–137, 1995.
[7] J. Craninckx and M. Steyaert, "A CMOS 1.8 GHz low-phase-noise voltage-controlled oscillator with prescaler," in *Int. Solid-State Circuits Conf.*, San Francisco, 1995, pp. 206–207.
[8] J. Min, A. Rofougaran, H. Samueli, and A. A. Abidi, "An all-CMOS architecture for a low-power frequency-hopped 900 MHz spread-spectrum transceiver," in *Custom IC Conf.*, San Diego, CA, 1994, pp. 379–382.
[9] A. A. Abidi, "Low-power radio-frequency IC's for portable communications," *Proc. IEEE*, vol. 83, no. 4, pp. 544–569, 1995.

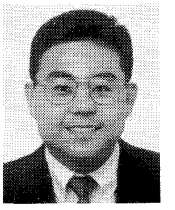
ParkerVision Exhibit 2032
TI v. ParkerVision - IPR2024-00934

[10] ——, "Direct-conversion radio transceivers for digital communications," *IEEE J. Solid-State Circuits*, vol. 30, no. 12, pp. 1399–1410, 1985.
[11] R. E. Lehmann and D. D. Heston, "X-band monolithic series feedback LNA," *IEEE Trans. Microwave Theory Tech.*, vol. MTT-33, no. 12, pp. 1560–1566, 1985.
[12] T. Okanobu, H. Tomiyama, and H. Arimoto, "Advanced low-voltage single chip radio IC," *IEEE Trans. Consumer Electron.*, vol. 38, no. 3, pp. 465–475, 1992.
[13] P. R. Gray and R. G. Meyer, *Analysis and Design of Analog Integrated Circuits*, 3rd ed. New York: Wiley, 1993.
[14] A. A. Abidi, "High frequency noise measurements on FET's with small dimensions," *IEEE Trans. Electron Devices*, vol. ED-33, pp. 1801–1805, 1986.
[15] M. Sakakura and S. Skiest, "Ultra-miniature chip inductors serve at high frequency," in *J. Electron. Eng.*, pp. 48–51, Dec. 1993.
[16] P. K. Ko, "Approaches to scaling," in *Advanced MOS Device Physics, VLSI Electronics: Microstructure Science*, N. G. Einspruch and G. S. Gildenblat Eds. San Diego, CA: Academic, vol. 18, p. 12, 1989.
[17] H. M. Greenhouse, "Design of planar rectangular microelectronic inductors," *IEEE Trans. Parts, Hybrids, Packag.*, vol. PHP-10, no. 2, pp. 101–109, 1974.
[18] N. M. Nguyen and R. G. Meyer, "A silicon bipolar monolithic RF bandpass amplifier," *IEEE J. Solid-State Circuits*, vol. 27, no. 1, pp. 123–127, 1992.
[19] J. N. Burghartz, M. Soyuer, K. A. Jenkins, and M. D. Hulvey, "High-Q inductors in standard silicon interconnect technology and its application to an integrated RF power amplifier," in *Int. Electron Devices Mtg.*, Washington, DC, 1995, pp. 29.8.1–29.8.3.
[20] S. A. Maas, *Microwave Mixers*, 2nd ed. Boston: Artech House, 1993.
[21] Y. P. Tsividis, "Integrated continuous-time filter design—An overview," *IEEE J. Solid-State Circuits*, vol. 29, no. 3, pp. 166–176, 1994.
[22] K. Bult and H. Wallinga, "A class of analog CMOS circuits based on the square-law characteristic of an MOS transistor in saturation," *IEEE J. Solid-State Circuits*, vol. SC-22, no. 3, pp. 357–365, 1987.
[23] R. G. Meyer and W. D. Mack, "A 1-GHz BiCMOS RF front-end IC," *IEEE J. Solid-State Circuits*, vol. 29, no. 3, pp. 350–355, 1994.
[24] N. Camilleri, J. Kirschgessner, J. Costa, D. Ngo, and D. Lovelace, "Bonding pad models for silicon VLSI technologies and their effects on the noise figure of RF NPN's," in *Microwave & Millimeter-Wave Monolithic Circuits Symp.*, San Diego, CA, 1994, pp. 225–228.
[25] C. Takahashi, R. Fujimoto, S. Arai, T. Itakura, T. Ueno, H. Tsurumi, H. Tanimoto, S. Watanabe, and K. Hirakawa, "A 1.9 GHz Si direct conversion receiver IC for QPSK modulation systems," in *Int. Solid-State Circuits Conf.*, San Francisco, 1995, pp. 138–139.
[26] TriQuint Semiconductor, "TQ9203J downconverter application note," p. 7, 1994.



Ahmadreza Rofougaran was born in 1964. He received the B.S. and M.S. degrees in electrical engineering from the University of California, Los Angeles, in 1986 and 1988, respectively. He is presently working toward the Ph.D. degree in the design of silicon IC's for RF communications at UCLA.

From 1988 to 1992 he was with Gigabit Logic, Inc., Newbury Park, CA, involved in the development of high-speed analog and digital GaAs IC's.



James Y.-C. Chang was born in Taiwan in 1968. He received the B.S. degree in electrical engineering (*magna cum laude*) from the University of California, Irvine, in 1990 and the M.S.E.E degree from the University of California, Los Angeles (UCLA), in 1992. He is currently working toward the Ph.D. degree at UCLA.

He received a patent for his M.S. work on large suspended spiral inductors in standard CMOS process, which he used to demonstrate the first CMOS RF tuned amplifier in 2-μm CMOS. His Ph.D. research is on the integration of a full CMOS RF front-end for a 900 MHz spread spectrum receiver. His research interests include high-speed analog integrated circuit design and communication systems.

Mr. Chang is a member of Eta Kappa Nu and Tau Beta Pi.



Maryam Rofougaran was born in 1968. She received the B.S. and M.S. degrees in electrical engineering from the University of California, Los Angeles, in 1991 and 1995, respectively.

She is presently involved in the research and design of high-speed CMOS analog integrated circuits at the IC&S Laboratory, University of California, Los Angeles.



Asad A. Abidi (S'75–M'80–SM'95–F'96) was born in 1956. He received the B.Sc. (Hon.) degree from Imperial College, London, in 1976 and the M.S. and Ph.D. degrees in electrical engineering from the University of California, Berkeley, in 1978 and 1981.

He was at Bell Laboratories, Murray Hill, NJ, from 1981 to 1984 as a Member of Technical Staff in the Advanced LSI Development Laboratory. Since 1985, he has been at the Electrical Engineering Department of the University of California, Los Angeles where he is Professor. He was a Visiting Faculty Researcher at Hewlett Packard Laboratories during 1989. His research interests are in CMOS RF design, high-speed analog integrated circuit design, data conversion, and other techniques of analog signal processing.

Dr. Abidi served as the Program Secretary for the International Solid-State Circuits Conference from 1984 to 1990, and as General Chairman of the Symposium on VLSI Circuits in 1992. He was Secretary of the IEEE Solid-State Circuits Council from 1990 to 1991, and from 1992 to 1995 he was Editor of the IEEE JOURNAL OF SOLID-STATE CIRCUITS. He received the 1988 TRW Award for Innovative Teaching.

ParkerVision Exhibit 2032
TI v. ParkerVision - IPR2024-00934